A Kinetic Model of Single and Clustered IP_3 Receptors in the Absence of Ca^{2+} Feedback

Jianwei Shuai,* John E. Pearson,† J. Kevin Foskett,‡ Don-On Daniel Mak,‡ and Ian Parker*
*Department of Neurobiology and Behavior, University of California, Irvine, California; †Theoretical Biology and Biophysics, Los Alamos National Laboratory, Los Alamos, New Mexico; and ‡Department of Physiology, University of Pennsylvania, School of Medicine, Philadelphia, Pennsylvania

ABSTRACT Ca^{2+} liberation through inositol 1,4,5-trisphosphate receptor (IP_3R) channels generates complex patterns of spatiotemporal cellular Ca^{2+} signals owing to the biphasic modulation of channel gating by Ca^{2+} itself. These processes have been extensively studied in *Xenopus* oocytes, where imaging studies have revealed local Ca^{2+} signals ("puffs") arising from clusters of IP_3R, and patch-clamp studies on isolated oocyte nuclei have yielded extensive data on IP_3R gating kinetics. To bridge these two levels of experimental data, we developed an IP_3R model and applied stochastic simulation and transition matrix theory to predict the behavior of individual and clustered IP_3R channels. The channel model consists of four identical, independent subunits, each of which has an IP_3-binding site together with one activating and one inactivating Ca^{2+}-binding site. The channel opens when at least three subunits undergo a conformational change to an "active" state after binding IP_3 and Ca^{2+}. The model successfully reproduces patch-clamp data; including the dependence of open probability, mean open duration, and mean closed duration on $[IP_3]$ and $[Ca^{2+}]$. Notably, the biexponential distribution of open-time duration and the dependence of mean open time on $[Ca^{2+}]$ are explained by populations of openings involving either three or four active subunits. As a first step toward applying the single IP_3R model to describe cellular responses, we then simulated measurements of puff latency after step increases of $[IP_3]$. Assuming that stochastic opening of a single IP_3R at basal cytosolic $[Ca^{2+}]$ and any given $[IP_3]$ has a high probability of rapidly triggering neighboring channels by calcium-induced calcium release to evoke a puff, optimal correspondence with experimental data of puff latencies after photorelease of IP_3 was obtained when the cluster contained a total of 40–70 IP_3Rs.

INTRODUCTION

The inositol 1,4,5-trisphosphate receptor (IP_3R) acts as a Ca^{2+} release channel to liberate Ca^{2+} ions from the endoplasmic reticulum (ER) into the cytosol (1). Structurally, the IP_3R is a large (~30 nm in diameter) homomeric tetramer of four subunits forming a single ion-conducting channel (2). Each subunit is composed of three functionally different domains, including a large cytoplasmic region of amino-terminal IP_3-binding domain, a carboxy-terminal channel-forming domain, and a middle coupling modulatory and transducing domain (3,4). Opening of the channel requires binding of the second-messenger inositol 1,4,5-trisphosphate (IP_3), which is generated in the cytoplasm in response to the binding of extracellular ligands to plasma membrane receptors. Moreover, gating of the IP_3R is biphasically modulated by Ca^{2+} ions, such that small elevations of cytosolic $[Ca^{2+}]$ promote channel opening, whereas higher $[Ca^{2+}]$ results in inactivation (5). This Ca^{2+} feedback underlies a process of Ca^{2+}-induced Ca^{2+} release (CICR), resulting in regenerative liberation of Ca^{2+} that may either remain restricted to a cluster of IP_3R to generate a localized Ca^{2+} puff (6), or propagate as a saltatory wave across numerous puff sites by successive cycles of Ca^{2+} diffusion and CICR.

To elucidate the complex spatiotemporal patterns of Ca^{2+} signals generated by the IP_3 pathway, we need to understand the functioning of IP_3Rs at the single-molecule level, the spatial arrangement of these receptors in the cell, and their functional interactions via Ca^{2+} diffusion and CICR. The *Xenopus* oocyte provides a favorable cell system with which to investigate these topics, by virtue of the wealth of experimental data available regarding both the imaging of IP_3-evoked Ca^{2+} signals in the intact cell (6–8) and patch-clamp recordings of single IP_3Rs in the outer membrane of isolated oocyte nuclei (9–12). To bridge these two levels of experimental data, we developed an IP_3R model, and used both transition matrix theory and stochastic simulation to predict the behavior of individual and clustered channels.

Models of the IP_3R play a central role not only for the understanding channel kinetics, but also as building blocks for constructing larger-scale models of cellular Ca^{2+} signaling. Several IP_3R models (13–19) have been developed to describe experimental data obtained from IP_3R reconstituted in bilayer membranes, with broad application of the DeYoung-Keizer model (14) in particular. However, there are significant differences in behavior of the reconstituted IP_3Rs versus that of IP_3Rs in their native environment of the nuclear envelope, and only a few models have incorporated IP_3R data obtained on nucleus membranes. Among these, an allosteric four-plus-two-conformation model was considered by Mak et al. (11). That model postulates that each of the four IP_3R monomers has one IP_3-binding site and three

Submitted March 12, 2007, and accepted for publication April 25, 2007.

Address reprint requests to Dr. Jianwei Shuai, Dept. of Neurobiology and Behavior, University of California, Irvine, CA 92697-4550. Tel.: 949-824-7833; Fax: 949-824-2447; E-mail: shuaij@uci.edu.

Editor: Raimond L. Winslow.

0006-3495/07/08/1151/12 $2.00

doi: 10.1529/biophysj.107.108795

different functional Ca^{2+}-binding sites on the cytoplasmic side of the channel. Another model was developed by Baran (20), consisting of one activation module and one inhibition module, both allosterically operated by Ca^{2+}, IP_3, and ATP, together with one adaptation module, driven by IP_3 and Ca^{2+}. However, these two models can predict only the steady-state gating properties, and not the kinetics of individual channel openings and closings.

Thus, there has been no model that could realistically simulate the kinetic behavior of IP_3R under physiological conditions in the *Xenopus* oocyte. Our aim was to develop a dynamic IP_3R model that successfully reproduces data obtained from patch-clamp recordings of nuclear IP_3Rs, and that is sufficiently simple and computationally tractable for application in future studies simulating the interactions of numerous IP_3Rs coupled in a cellular environment by Ca^{2+} diffusion and CICR. The channel model consists of four identical, independent subunits, each of which has an IP_3-binding site, together with one activating and one inactivating Ca^{2+} binding site. A feature of the model is that channel opening may occur if either three or four of the subunits of the tetramer are in an ''activated'' state (binding both IP_3 and the activating Ca^{2+} ion, but not the inhibitory Ca^{2+} ion), and we show how this characteristic can account for the observed biexponential distribution of open times and the dependence of mean open time on $[Ca^{2+}]$. Moreover, we extend our IP_3R channel model to the cellular level by simulating the latency of puffs after step increases of IP_3, on the assumption that the stochastic opening of a single IP_3R within a cluster rapidly evokes CICR from neighboring channels with high probability to generate a puff. On this basis, we predict that puff sites contain a total of 40–70 IP_3Rs.

MODEL

A schematic picture of the IP_3R model is shown in Fig. 1, which, from structural studies (2), comprises four identical and independent subunits. Based on experimental observations that the channel open probability is a bell-shaped function of $[Ca^{2+}]$ (5,10,15), we consider two independent Ca^{2+}-binding sites for each subunit; i.e., an activating binding site and an inhibitory site. Consistent with the molecular structure of the IP_3R (3,4) and concordant with most previous IP_3R models, we also assume a single IP_3 binding site in each subunit. The state of each subunit is denoted as (*ijk*), where the index *i* represents the IP_3-binding site, *j* the activating Ca^{2+}-binding site, and *k* the inhibitory Ca^{2+}-binding site. An occupied site is represented as 1, and a nonoccupied site as 0.

The model further includes a conformational change whereby a subunit in the (110) state (one IP_3 and one activating Ca^{2+} bound) is ''inactive'', and must transition to an ''active'' (A) state before it can contribute to channel opening. This conformational step is analogous to the well-characterized behavior of nicotinic acetylcholine receptors (21), and further implies that the active state is ''locked'' with respect to agonist binding and dissociation. Observations of ligand-independent flickerings of the IP_3R channel to the closed state (11) are consistent with such a conformational change, and the lack of effect of changes in Ca^{2+} concentration on gating of already open IP_3R channels (22) supports the notion that active subunits are locked with respect to ligand binding.

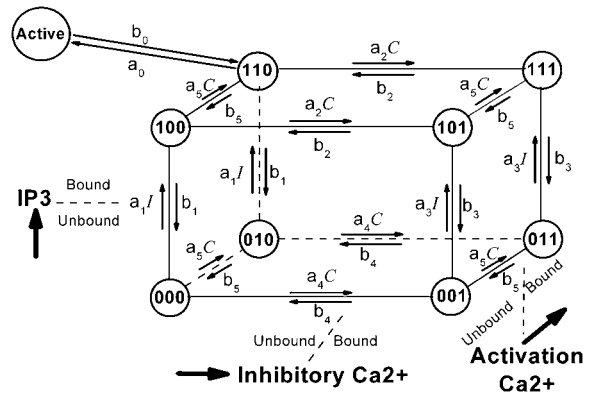

FIGURE 1 Schematic diagram of the model of a single IP_3R channel subunit. Each subunit has an activation Ca^{2+}-binding site, an inhibitory Ca^{2+}-binding site, and an IP_3-binding site. We label the binding sites by the notation (*ijk*), where the index *i* represents the IP_3-binding site, *j* the activation Ca^{2+}-binding site, and *k* the inhibitory Ca^{2+}-binding site. The number 1 represents an occupied binding site and 0 a nonoccupied site. Additionally we introduce a conformational change between ''active'' (A-state) and ''inactive'' (110) states of the subunit. Values for the forward (*a*) and backward (*b*) rate constants associated with each transition are listed in Table 1. In the figure, *C* and *I* represent the concentrations of Ca^{2+} and IP_3, respectively. The bold arrows indicate the binding of ligands to different sites.

We also assume that the channel is open when either three or four subunits are in an active state. This assumption has previously been applied in some IP_3R models (23), and we show here that it can explain the dependence of channel open time on ligand concentration. Although some multimeric channels show distinct conductance levels associated with ligand binding to differing numbers of subunits (24), the *Xenopus* oocyte IP_3R displays only a single major conductance level (11,12), so we distinguish only a single open state, irrespective of whether three or four subunits are active.

Each subunit in the model has nine states, with transitions governed by second-order rate constants (a_i, with $i > 0$) for binding processes, first-order rate constants (b_i, with $i > 0$) for unbinding process, and constant transition rates (a_0 and b_0) applied between the active A-state and the inactive (110) state (Fig. 1). Parameter values used in the model are listed in Table 1. Values for dissociation constants were chosen on the basis of optimal fit to steady-state experimental data from patch-clamped oocyte nuclear IP_3R (Fig. 2). For all the binding/unbinding loops given in Fig. 1, the thermodynamic constraint of detailed balance requires that $K_1K_2 = K_3K_4$ for reaction dissociation constants. The conformation rate changes a_0 and b_0 between the (110) and active states of

TABLE 1 Parameter values used in the IP_3R channel model

	Parameter	Value (unit)
Conformation change rate	a_0	540 s^{-1}
	b_0	80 s^{-1}
IP_3-binding site	K_1	0.0036 μM
	a_1	60 μM^{-1} s^{-1}
	K_3	0.8 μM
	a_3	5.0 μM^{-1} s^{-1}
Activating calcium-binding site	K_5	0.8 μM
	a_5	150 μM^{-1} s^{-1}
Inhibitory calcium-binding site	K_2	16 μM
	a_2	0.2 μM^{-1} s^{-1}
	K_4	0.072 μM
	a_4	0.5 μM^{-1} s^{-1}

In the table, the disassociation constant $K_i = b_i/a_i$, with a_i the on-binding rate and b_i the off-binding rate. Due to the thermodynamic constraint, we have $K_1K_2 = K_3K_4$.

the subunits were chosen to give a maximum channel open probability of ~0.84, as observed experimentally for *Xenopus* oocyte nuclei (10,11). The rate constant for IP_3 binding was based on experimental measurements of first opening latencies of 0.35 and 0.5 s for IP_3R channels in Sf9 cell nuclei at $[Ca^{2+}] = 2$ μM after step increases in $[IP_3]$ from 0 to 10 and 100 μM, respectively (K. Foskett and D. O. Mak; unpublished data). Model simulations of single channel latencies provided a good fit, with predicted corresponding mean latencies of 0.34 and 0.4 s. Rate constants for Ca^{2+} binding were estimated by iterative fitting of model predictions to published data of *Xenopus* oocyte IP_3R open- and closed-time distributions (10,11).

We explored the behavior of the IP_3R model using both deterministic, matrix transition analysis and stochastic simulation. The deterministic approach provides a rigorous analysis of statistical channel behavior, but cannot reveal the trajectory of openings and closings of an individual IP_3R. Because we wish to use the model as a building block to explore the contribution of stochastic single-channel behavior to cellular Ca^{2+} signaling, we also performed stochastic simulations; an approach that has the further advantage of providing a more intuitive insight into channel behavior.

Deterministic analysis of the IP_3R model

The probability of subunits in state (*ijk*) or (A) is denoted by P_{ijk} or P_A, with $P_A + \sum P_{ijk} = 1$. By the mass action kinetics, the equations describing the subunit dynamics are written

$$\frac{dP}{dt} = PQ, \tag{1}$$

where Q is the generator matrix (25) of transition rates and P is the vector of probability of subunits. The open probability for an IP_3R is then given by

$$P_O = P_A^4 + 4P_A^3(1 - P_A), \tag{2}$$

Mathematically, the equilibrium state is defined by $dP/dt = 0$. The equilibrium vector w satisfies $wQ = 0$.

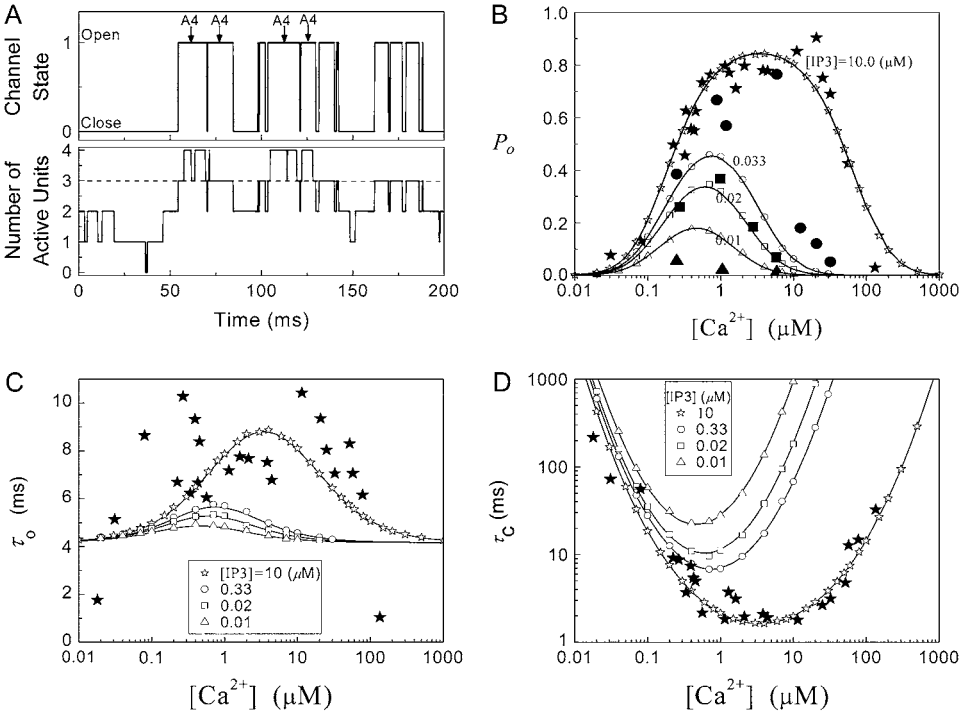

FIGURE 2 Stochastic and deterministic modeling of IP_3R dynamics, and comparison with steady-state experimental data. (*A*) Example of stochastic simulation of IP_3R channel gating (*upper*), and the corresponding numbers of subunits in the active state (*lower*) at $[IP_3] = 10$ μM and $[Ca^{2+}] = 0.2$ μM. Arrows mark openings that are associated with 4-related open states. (*B*) Graph shows the dependence of steady-state open probability (P_O) as a function of $[Ca^{2+}]$ for different concentrations of IP_3. Solid curves show results by the deterministic transition matrix theory. The results obtained by stochastic simulation are represented by open symbols ($[IP_3] = 10$ μM (*stars*), 0.033 μM (*circles*), 0.02 μM (*squares*), and 0.01 μM (*triangles*)). Single-channel patch-clamp experimental data obtained from IP_3R on native nuclear membranes by Mak et al. (10,11) were replotted as solid symbols ($[IP_3] = 10$ μM (*stars*); 0.033 μM (*circles*); 0.02 μM (*squares*); and 0.01 μM (*triangles*)). (*C* and *D*) Mean open time τ_O (*C*) and closed time τ_C (*D*), respectively, as functions of $[Ca^{2+}]$ for different concentrations of IP_3, as indicated. Solid curves show results obtained with transition matrix theory, and open symbols show stochastic simulation results. Solid stars show corresponding experimental data at $[IP_3] = 10$ μM (10,11).

Detailed balance is imposed so that we can solve for w by inspection (26). This is done by calculating all probabilities in terms of their probability relative to state (000). These unnormalized probabilities are denoted q_{ijk}, with $q_{0000} = 1$. Then

$$w_{\mathrm{ijk}} = \frac{q_{\mathrm{ijk}}}{Z}, \tag{3}$$

where each component (q_{ijk}/Z) gives the equilibrium probability for state (ijk). Z is the normalization factor defined by $Z = q_{\mathrm{A}} + \sum q_{\mathrm{ijk}}$. The equilibrium probability (q_{ijk}) of state (ijk) relative to that of state (000) is just the product of forward to backward rates along any path connecting (000) to (ijk). Thus, we can write

$$q_{\mathrm{A}} = \frac{[\mathrm{IP_3}] \times [\mathrm{Ca}^{2+}]}{K_1 K_5} \times \frac{a_0}{b_0}, \tag{4}$$

and

$$Z = \left(1 + \frac{[\mathrm{Ca}^{2+}]}{K_4}\right)\left(1 + \frac{[\mathrm{Ca}^{2+}]}{K_5}\right) + \frac{[\mathrm{IP_3}]}{K_1}\left(1 + \frac{[\mathrm{Ca}^{2+}]}{K_2}\right)\left(1 + \frac{[\mathrm{Ca}^{2+}]}{K_5}\right) + q_{\mathrm{A}}. \tag{5}$$

The equilibrium probability for the subunit active state is given by

$$w_{\mathrm{A}} = \frac{q_A}{Z} = \frac{[\mathrm{IP_3}] \times [\mathrm{Ca}^{2+}]}{K_1 K_5} \times \frac{a_0}{b_0} \times \frac{1}{Z}. \tag{6}$$

Since the channel is open if either three or four subunits are active, the equilibrium open probability is a sum of contributions from three and four active subunits: $p_3 = 4w_{\mathrm{A}}^3(1 - w_{\mathrm{A}})$ and $p_4 = w_{\mathrm{A}}^4$. Thus, the open probability at the equilibrium state for an $\mathrm{IP_3R}$ channel is

$$P_{\mathrm{O}} = w_{\mathrm{A}}^4 + 4w_{\mathrm{A}}^3(1 - w_{\mathrm{A}}). \tag{7}$$

Because channel states (A, A, A, not-A) are the only open states that connect to closed channel states by any one of three A-states changing to the closed state 110 with rate b_0, we can directly write the equilibrium probability flux between open and closed states as follows:

$$J = 3b_0 p_3. \tag{8}$$

The mean open and closed times are given by

$$\tau_{\mathrm{O}} = \frac{P_{\mathrm{O}}}{J} = \frac{1}{3b_0} \times \frac{P_{\mathrm{O}}}{p_3} = \frac{1}{3b_0} \times \left(1 + \frac{p_4}{p_3}\right)$$
$$\tau_{\mathrm{C}} = \frac{1 - P_{\mathrm{O}}}{J} = \frac{1}{3b_0} \times \frac{1 - P_{\mathrm{O}}}{p_3} \tag{9}$$

Equation 9 implies that the channel mean open time varies even though the subunit mean active time is fixed. τ_{O} has a limiting minimum value of $1/(3b_0)$ and increases as p_4/p_3 increases. This is to be expected since the channel is open if either three or four subunits are active but closes only when there are precisely three active subunits.

Deterministic solutions presented in Fig. 2 (showing the open probability P_{O}, mean open time τ_{O}, and mean closed time τ_C as functions of constant Ca^{2+} concentration at different $\mathrm{IP_3}$) were obtained using Eqs. 7 and 9. Furthermore, we applied the transition matrix theory to predict the open- and closed-time distributions of the channel in steady state and the distributions of the first-opening latency of individual and clustered $\mathrm{IP_3Rs}$ responding to step $\mathrm{IP_3}$ stimulus. The analytic deductions employed to obtain those results will be described in detail in a separate article (J. Shuai, I. Parker, and J. E. Pearson; unpublished).

Stochastic simulation of the $\mathrm{IP_3R}$ model

We simulated the stochastic dynamics of this nine-state subunit channel model by a Markov process (27,28), updating the state of the system at small time steps dt. For example, a channel subunit in the (110) state at time t could transition to states (010), (100), (111), or to the active A-state at the next time step $t + dt$ with respective transition probabilities of $b_1 dt$, $b_5 dt$, $a_2[\mathrm{Ca}^{2+}] \times dt$, or $a_0 dt$; otherwise, it remains in the same state. Random numbers homogeneously distributed in $[0,1]$ were generated at each time step and compared with these transition probabilities to determine the state of the channel subunit at the next time step. The $\mathrm{IP_3R}$ channel is open when three or four subunits are in the A-state. A time step $dt = 10\ \mu\mathrm{s}$ was generally used, being much shorter than mean channel open or closed times. The results were not appreciably different when dt was altered between 0.1 and 50 μs, and the close correspondence obtained with results of the deterministic analysis further validates the simulation method.

RESULTS

Steady-state $\mathrm{IP_3R}$ dynamics

In this section, we describe the behavior of the single $\mathrm{IP_3R}$ model under steady-state conditions of given $[\mathrm{IP_3}]$ and $[\mathrm{Ca}^{2+}]$, and demonstrate that our model successfully reproduces the experimental data obtained from patch-clamped $\mathrm{IP_3R}$ on the *Xenopus* oocyte nuclear membrane (9–12).

An example of stochastic channel gating

Fig. 2 *A* illustrates stochastic channel gating, and the corresponding subunit states under conditions $[\mathrm{IP_3}] = 10$ μM and $[\mathrm{Ca}^{2+}] = 0.2$ μM that result in a mean open probability (P_{O}) of ~0.4. Because the channel opens when either three or four subunits are active, we can distinguish two different types of channel open state: A3-only openings and A4-related openings. We define A3-only openings as those involving only three simultaneously active subunits throughout the duration of the opening, whereas A4-related

openings involve at least one occurrence of all four subunits being active (e.g., openings marked by *arrows* in Fig. 2 *A*).

Dependence of open probability on $[IP_3]$ and $[Ca^{2+}]$

The solid symbols in Fig. 2 *B* show experimental measurements from oocyte nuclei of the dependence of IP_3R channel open probability (P_O) as a function of cytosolic $[Ca^{2+}]$ for different concentrations of IP_3 (10,11). The data follow the well-known ''bell-shape'' distribution, with increasing concentrations of IP_3 producing a rightward shift in the Ca^{2+} concentration required for maximal P_O, and with the maximal P_O increasing steeply for IP_3 concentrations between 10 and 33 nM. These experimental observations are fit reasonably well by our IP_3R model, as shown in Fig. 2 *B* by results obtained from both deterministic analysis (*solid curves*) and stochastic simulation (*open symbols*). An exception is that the model predicts a less steep dependence of P_O at low values of $[IP_3]$ than was experimentally observed.

A maximal $P_O = 0.84$ was achieved with the model under optimal conditions ($[IP_3] > 0.5\ \mu M$ and $[Ca^{2+}] \approx 3\ \mu M$). This corresponds well with measurements from IP_3R on the *Xenopus* oocyte nucleus (10,11), but is much greater than that ($P_O \approx 0.2$) observed for cerebellar IP_3R reconstituted in lipid bilayers (5). Concentrations of $IP_3 > \sim 0.5\ \mu M$ are already saturating, as expected from the relatively high binding affinity ($K_1 = 0.0036\ \mu M$) in the model.

Mean open and closed time

The mean open (τ_O) and closed (τ_C) times of the IP_3R channel are plotted, respectively, in Fig. 2, *C* and *D*, as functions of Ca^{2+} and IP_3 concentrations for the deterministic (*solid curves*) and stochastic (*open symbols*) versions of the IP_3R model, together with experimental data (*solid symbols*) from oocyte nuclear receptors at $[IP_3] = 10\ \mu M$ (10). It is evident that the dependence of P_O upon $[Ca^{2+}]$ and $[IP_3]$ described in Fig. 2 *B* arises primarily through correspondingly large changes in τ_C, and the model results with 10 μM IP_3 fit well to the experimental observations. Additionally, although subject to appreciable scatter, the patch-clamp data also reveal a modest (two- to threefold) increase in τ_O associated with increasing P_O (10). This behavior is reproduced by our model (Fig. 2 *C*).

Variation of mean open time on $[IP_3]$ and $[Ca^{2+}]$

At first sight, the dependence of predicted τ_O on ligand concentrations (Fig. 2 *C*) appears unexpected, given that the transition rate b_0 from the active A-state to the closed state (1110) of each subunit is a fixed value, resulting in a constant active dwell time of $1/b_0$ for each subunit. Theory (Eq. 9) indicates that mean open time τ_O varies with $[Ca^{2+}]$ and $[IP_3]$ because the probability for being in the gateway states in which three subunits are active varies with respect to being in the single state with four active subunits. Indeed, the theory is in solid accord with the experimental data, in which the mean open time varies by about a factor of 2. The variation in τ_O is given by the factor $1 + p_3/p_4 = 1 + w_A/(4(1 - w_A))$ (see Eq. 9). The IP_3R is observed to have a maximum P_O of ~ 0.84. To within a few percent, P_O takes on its maximum value of 0.84 when w_A is ~ 0.8. This occurs when $p_3 = p_4$. Thus, theory predicts that the channel mean open time varies by a factor of 2, in accord with observation. To further illustrate this point, we analyzed the results of stochastic simulations, and we show below that the variation in mean open time results because there are two populations of channel open states, involving only three simultaneously active subunits, or at least one occurrence of four active subunits.

We first determined the mean open times associated with each of these conformations. Fig. 3 *A* shows that mean open times for A3-only openings (T_3) and for A4-related openings (T_4) change only slightly as a function of $[Ca^{2+}]$ at $[IP_3] = 10\ \mu M$, with respective values of $\sim$2.6–4.2 and 14.5–15.5 ms. The mean open time T_{A3} can be intuitively understood

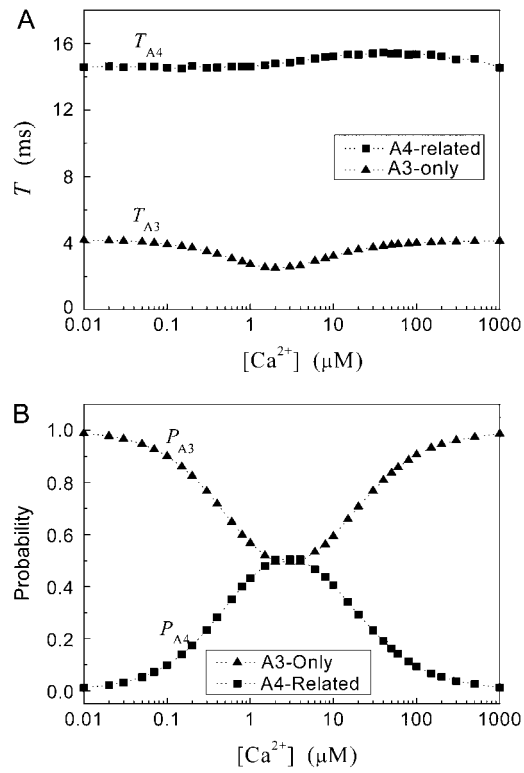

FIGURE 3 Dependence of τ_O on ligand concentration can be explained by a change in the proportion of openings involving only three active subunits (A3-only openings) and those involving four active subunits (A4-related openings). (*A*) Stochastic simulation results demonstrating that the mean open times of A3-only and A4-related openings show only a slight dependence on $[Ca^{2+}]$ for $[IP_3] = 10\ \mu M$. (*B*) The probabilities of A3-only and A4-related openings as functions of $[Ca^{2+}]$. In both panels, $[IP_3] = 10\ \mu M$.

because the channel will close when any one of the three active subunits becomes inactive, so that $T_{A3} \approx 1/(3b_0) \approx$ 4 ms.

Because the mean dwell times of A3- only and A4-related openings have only a slight ligand dependence, the change in mean channel open time with ligand concentration must, therefore, involve also a change in proportion of A3- only and A4-related events. For example, with $[Ca^{2+}]$ at an optimal value of $\sim 3\ \mu M$, each subunit will have a high probability of being in the active state, thereby increasing the probability of finding four active subunits; whereas at lower $[Ca^{2+}]$ the probability of subunits having Ca^{2+} bound to the activating site is lower, and at higher $[Ca^{2+}]$ there is an increasing chance of subunits becoming inhibited. Thus, the probability for A4-related openings, P_{A4}, first increases and then decreases with increasing $[Ca^{2+}]$, and the probability for A3-only openings, P_{A3}, correspondingly follows an inverse relationship (Fig. 3 *B*).

The mean open time of the channel, expressed as

$$\tau_O = P_{A3}T_{A3} + P_{A4}T_{A4}, \tag{10}$$

therefore varies as a function of $[Ca^{2+}]$ and $[IP_3]$. At very low and high $[Ca^{2+}]$, the mean open time τ_O derives almost entirely from the A3-only open state, giving a value of $\tau_O \approx 4$ ms. At the optimal value of $[Ca^{2+}]$, $\sim 3\ \mu M$, $P_{A3} \approx P_{A4} = 0.5$ (Fig. 3 *B*), so that $\tau_O \approx 0.5 \times (T_{A3} + T_{A4}) \approx 9$ ms.

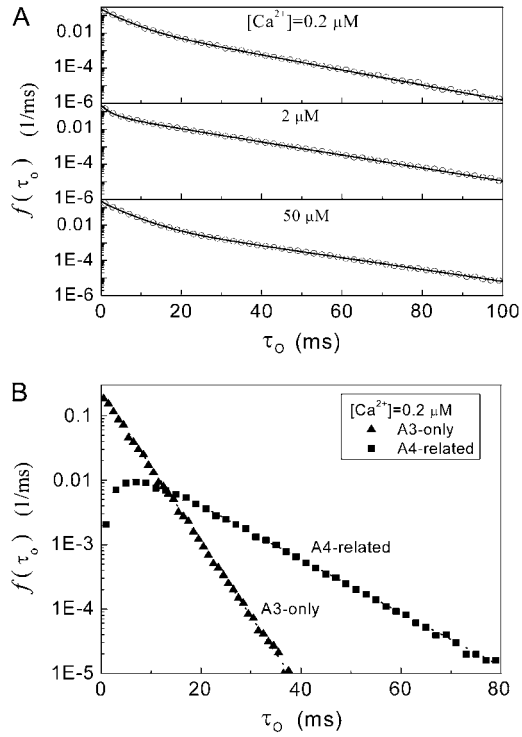

FIGURE 4 Distributions of open times predicted by the IP_3R channel model. (*A*) Open-time distributions for basal Ca^{2+} concentrations at $[Ca^{2+}] = 0.2$, 2, and 50 μM with $[IP_3] = 10\ \mu M$. Open symbols are results of stochastic simulations, and solid curves were obtained from the transition matrix theory. (*B*) Distributions of channel open durations involving A3-only and A4-related openings, derived from stochastic modeling at $[Ca^{2+}] = 0.2\ \mu M$ and $[IP_3] = 10\ \mu M$.

Open- and closed-time distributions

Patch-clamp experimental data show that open-channel dwell times follow a biexponential distribution, with time constants of ~4 ms and 20 ms (12). This behavior is predicted also by our model with stochastic simulation and deterministic theory, where the open-time distributions at various $[Ca^{2+}]$ are approximated by a sum of two exponentials (Fig. 4 *A*). These two exponential components can be considered as arising from A3-only and A4-related openings. For example, the distributions of A3-only and A4-related open dwell times are plotted in Fig. 4 *B* for $[Ca^{2+}] = 2\ \mu M$ and $[IP_3] = 10\ \mu M$. The distribution of A3-only openings is monoexponential, with a time constant of ~4 ms, and the distribution of A4-related openings approximates an exponential with time constant of ~12 ms for openings >10 ms. For various $[Ca^{2+}]$ at $[IP_3] = 10\ \mu M$, time constants of A3-only and A4-related exponential open distribution are ~3–5 and 9–14 ms, respectively.

Patch-clamp experimental data show that the IP_3R channel has at least two closed states, with the time constants ~1 ms and 10 ms, as well as a long closed kinetic state with time constant of the order of seconds (12). Our model predicts also a rich kinetic behavior for closed dwell times. Three examples of closed-time distributions are plotted in Fig. 5 *A* for $[Ca^{2+}] = 0.2$, 2.0, and 200 μM at $[IP_3] = 10\ \mu M$. For $[Ca^{2+}] = 0.2\ \mu M$ (Fig. 5 *A*, *upper*), three exponential components can be clearly distinguished at regions $\tau_C < 10$ ms, $20 < \tau_C < 400$ ms, and $\tau_C > 450$ ms, with time constants of 1, 25, and 160 ms, respectively. For $[Ca^{2+}] = 2.0$ and 200 μM, the distributions can be approximated by two exponential functions: a fast component with time constant 1–3 ms and a slow component with time constants 200–300 ms. The faster component (time constant ~2 ms) derives largely from immediate, ligand-independent transitions from the (110) state of the model to the active state, as set by the time constant $1/a_0$. The slower components derive from transitions involving the other seven closed states, and are expected to be correspondingly complex. In practice, we are able to discern only a maximum of three-exponential functions by fitting to predicted closed-time distributions.

The multiexponential distributions of closed times lead to a ''burst-like'' behavior of channel gating. During bursts of rapid openings, short closings arise largely as any one of three active subunits undergoes round-trip transitions through the (110) states, whereas the more prolonged interburst intervals result from subunits entering longer-lived inactive states that require ligand association or dissociation to return to the (110) state. A running average of instantaneous P_O with a time

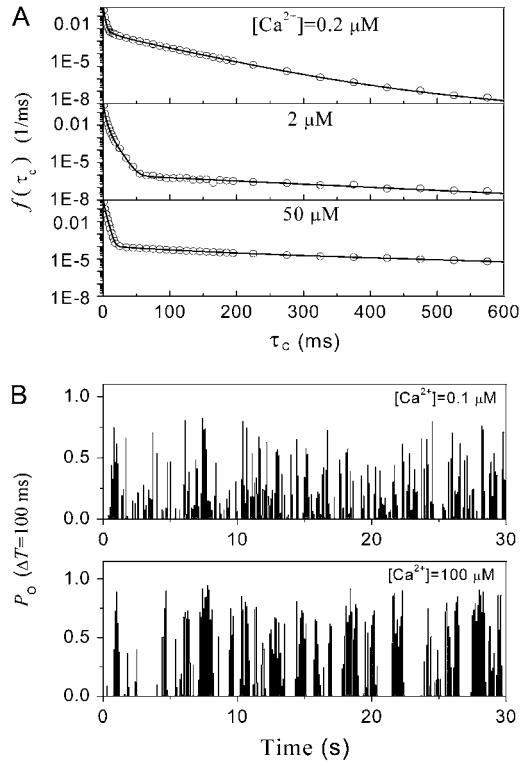

FIGURE 5 Multicomponent closed-time distributions of the IP_3R channel result in ''burst-like'' behavior. (*A*) Closed-time distributions at $[Ca^{2+}] = 0.2$, 2.0, and 50 μM for $[IP_3] = 10$ μM. Open symbols are stochastic simulations and solid curves are from the transition matrix theory. (*B*) Two examples of the fluctuation in average channel open probability within a 100-m-running window, respectively, for $[Ca^{2+}] = 0.1$ and 100 μM and $[IP_3] = 10$ μM.

window of 100 ms thus shows large fluctuations over time (Fig. 5 *B*), similar to that observed experimentally (12).

Puff latencies after steps of $[IP_3]$

In this article, we limit consideration of our IP_3R model to conditions where $[Ca^{2+}]$ is fixed at given values. The results are therefore not immediately applicable to cellular signaling, where cytosolic $[Ca^{2+}]$ fluctuates widely owing to Ca^{2+} flux through the IP_3Rs themselves. An exception, however, concerns experimental observations of Ca^{2+} puffs evoked by flash photorelease of IP_3, where the mean puff latency shortens with increasing $[IP_3]$ (7,8). In this case, the basal cytosolic $[Ca^{2+}]$ remains essentially unchanged before the puff, permitting us to simulate puff initiation by considering the stochastic variability in opening of an IP_3R channel after a step increase in $[IP_3]$ at constant $[Ca^{2+}]$. We assume that opening of a single IP_3R channel provides sufficient ''trigger'' Ca^{2+} to activate neighboring channels and thereby evoke a puff (29), and estimate the number of IP_3R clustered at a puff site by fitting the stochastic simulation results to experimental data.

Responses of a single IP_3R channel to a step of $[IP_3]$

We first consider the latency of an individual channel after a step increase in IP_3 concentration. Initially, the channel is in equilibrium at biologically realistic resting conditions with cytosolic $[Ca^{2+}]_{Rest} = 0.1\,\mu M$ and $[IP_3] = 0$ μM. At time $t = 0$, the concentration of IP_3 increases instantaneously from 0 μM to $[IP_3]_{Stim}$ to simulate the rapid photorelease of IP_3 by an ultraviolet flash. Examples of three responses to a step $[IP_3]_{Stim} = 10$ μM are presented in Fig. 6 *A*, illustrating the stochastic variability in channel kinetics. Here, we are concerned only with the latency to the first opening of the channel, and disregard subsequent openings. Fig. 6, *B* and *C*, plots distributions of channel first-opening latencies for various $[IP_3]_{Stim}$ and $[Ca^{2+}]_{Rest}$ obtained from simulation and theory. The distributions follow skewed $\cap$-shaped curves that shift leftward and become narrower with increasing $[IP_3]_{Stim}$ (Fig. 6 *B*) and $[Ca^{2+}]_{Rest}$ (Fig. 6 *C*).

The mean first-opening latency of the channel as a function of $[IP_3]_{Stim}$ is shown in Fig. 7 *A* for $[Ca^{2+}]_{Rest} = 0.1$ μM. The latency shortens markedly as $[IP_3]_{Stim}$ increases from 0 to 5 μM, but then reaches a minimum value of ~400 ms at higher $[IP_3]_{Stim}$. The mean first-opening latency of the channel as a function of $[Ca^{2+}]_{Rest}$ is shown in Fig. 7 *C* for $[IP_3]_{Stim} = 0.1$ and 10 μM. An interesting observation is that changes in $[Ca^{2+}]_{Rest}$ from 0.05 to 0.2 μM cause an increase of the mean minimum latency at low $[IP_3]_{Stim}$ (from ~2500 to ~3500 ms for $[IP_3]_{Stim} = 0.1$ μM), but a decrease of the latency at high $[IP_3]_{Stim}$ (from ~650 to ~350 ms for $[IP_3]_{Stim} = 10$ μM).

These results can be understood in terms of the states of the IP_3R subunit model. For very small $[Ca^{2+}]_{Rest}$ (≤ 0.01 μM), >85% channel subunits are in the (000) state at $[IP_3] = 0$ μM. The binding of Ca^{2+} becomes rate-limiting, so that the latencies are long and have little dependence on $[IP_3]_{Stim}$. At physiological cytosolic $[Ca^{2+}]_{Rest}$ (~0.1 μM), an important result is that a large proportion of subunits are predicated to be in a Ca^{2+}-inhibited state (e.g., at $[Ca^{2+}] = 0.2$ μM and $[IP_3] = 0$ μM, 75% of subunits are in the (001) or (011) states) before flash photorelease of IP_3. As a result, changes in basal $[Ca^{2+}]_{Rest}$ will have dual opposing effects on the latency, with increasing $[Ca^{2+}]_{Rest}$ both increasing the steady-state probability of subunits being in Ca^{2+}-inhibited states, and also speeding the binding of Ca^{2+} to the activating site. At physiological cytosolic $[Ca^{2+}]_{Rest}$, our model shows that these two effects function differently at different $[IP_3]_{Stim}$. In particular, a fourfold change in $[Ca^{2+}]_{Rest}$ from 0.05 to 0.2 μM results in a small shortening of the mean latency for large $[IP_3]_{Stim}$ and a small lengthening of the mean latency for small $[IP_3]_{Stim}$ (Fig. 7 *C*).

Responses of clustered IP_3Rs to steps of $[IP_3]$

We next extend our simulation from a single IP_3R channel to a cluster of *N* functionally independent channels representing

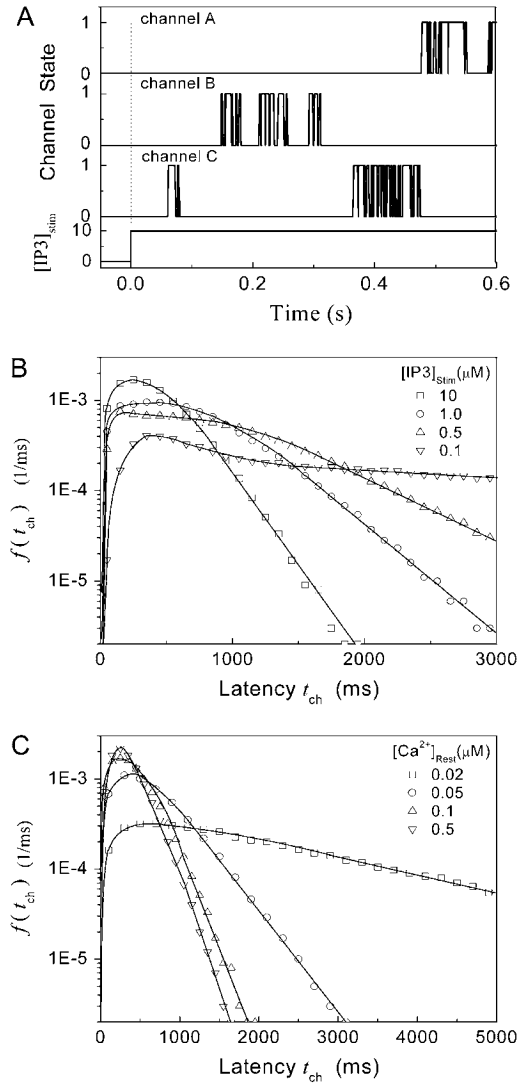

FIGURE 6 Distributions of first-opening latencies for a single IP_3R after different steps of $[IP_3]$ at various $[Ca^{2+}]$. (*A*) Three examples are shown of stochastic simulations for a step of $[IP_3]$ from 0 to 10 μM (*lower*) with $[Ca^{2+}] = 0.1$ μM. (*B* and *C*) Distributions of first-opening latencies after stepwise increases in $[IP_3]$ derived from stochastic modeling (*open symbols*) and theory (*solid lines*). Results are plotted for different magnitudes of $[IP_3]_{Stim}$ with $[Ca^{2+}] = 0.1$ μM (*B*), and for different $[Ca^{2+}]$ with $[IP_3]_{Stim} = 10$ μM (*C*).

a puff site. Again, the channels are equilibrated at the resting condition ($[Ca^{2+}]_{Rest} = 0.1$ μM and $[IP_3] = 0$ μM), and a step of $[IP_3]$, i.e., $[IP_3]_{Stim}$, is imposed at time $t = 0$. We initially assume that opening of a single channel invariably triggers a puff by CICR, so that the puff latency, T_{Puff}, is the interval from $t = 0$ to the first opening of any channel in the cluster. We then explore the effect of reducing the probability of puff initiation by opening of a single channel.

The mean puff latency T_{Puff} is plotted as a function of $[IP_3]_{Stim}$ and $[Ca^{2+}]_{Rest}$ in Fig. 7, *B* and *D*, respectively, for clusters of $N = 50$ channels. In comparison with the first-opening latency of a single IP_3R, the T_{Puff} is ~5–10 times shorter for a given $[IP_3]_{Stim}$—as expected, since it represents the first among the 50 channels to open—but the general shape of the curve is similar.

An interesting observation is that the mean latency for clustered IP_3Rs for both large and small $[IP_3]_{Stim}$ at first shortens as $[Ca^{2+}]_{Rest}$ is raised from a low value (0.005 μM), but reaches a minimum at ~0.1 μM and thereafter actually shows a slight lengthening (Fig. 7 *D*). An explanation is that binding of Ca^{2+} to activating sites is rate-limiting at very low $[Ca^{2+}]_{Rest}$, so that the latency first becomes shorter as $[Ca^{2+}]_{Rest}$ increases from 0.01 μM. However, at higher concentrations (>0.1 μM), there is an increasing likelihood of subunits being in an inhibited state due to $K_4 = 0.072$ μM (Fig. 1), so that the latency approaches a minimal value set by the dissociation rate b_2 from inhibitory Ca^{2+}-binding sites.

Fig. 8 *A* shows the puff latency distributions obtained from theory and simulation for $[IP_3]_{Stim} = 10$ μM and $[Ca^{2+}]_{Rest} = 0.1$ μM considering clusters containing $N = 25$, 50, and 150 channels. The curves represent the stochastic variability in first-opening latencies, and since they reflect the population behavior of multiple channels, the peaks of the distributions shift to shorter latencies with increasing N while the spread of the distribution narrows.

Number of IP_3Rs at a puff site

To compare model predictions with the experimental data, the mean puff latency T_{Puff} is replotted as a function of $1/[IP_3]_{Stim}$ in Fig. 8 *B* for clusters of $N = 25$, 50, and 150 channels at $[Ca^{2+}]_{Rest} = 0.1$ μM, together with experimental data of puff latencies in *Xenopus* oocytes taken from Callamaras et al. (7) and Parker et al. (8). The experimental puff latency T_{Exp} can be fit as a linear function of $1/[IP_3]_{Stim}$ (7),

$$T_{Exp}(I_{Stim}) = T_0 + \frac{k}{I_{Stim}}, \tag{11}$$

with the minimal latency $T_0 = 41$ ms and slope $k = 16.5\,\text{ms}\times\mu\text{M}$ (Fig. 8 *B*, *solid line*). Good agreement with these experimental data was obtained by simulating a cluster containing 50 IP_3R channels.

To better quantify the agreement between model and experimental measurements of puff latencies (T_{Model} and T_{Exp}, respectively), we introduce an optimal matching function:

$$\Theta(N, [Ca^{2+}]_{Rest}) = -lg(\Phi(N, [Ca^{2+}]_{Rest})), \tag{12}$$

with

$$\Phi = \frac{1}{M}\sum_{[IP_3]_{Stim}=I_1}^{I_M}\left(\frac{T_{Model}(N, [IP_3]_{Stim}) - T_{Exp}([IP_3]_{Stim})}{T_{Exp}([IP_3]_{Stim})}\right)^2. \tag{13}$$

A larger value of Θ indicates a better match between the modeled puff and the experimental observation.

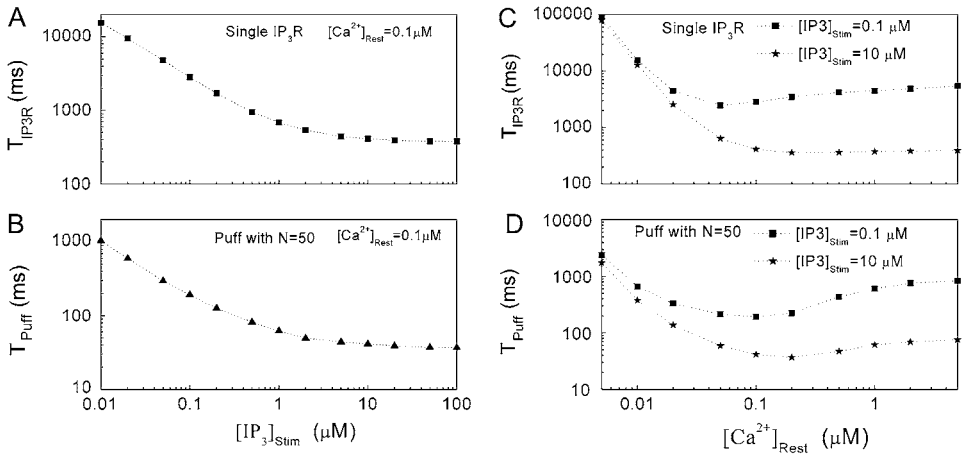

FIGURE 7 Mean first-opening latencies for single and multiple IP_3R after different steps of $[IP_3]_{Stim}$ at various $[Ca^{2+}]$. (*A* and *B*) The mean first-opening latency of an individual IP_3R channel (*A*) as a function of $[IP_3]_{Stim}$, with $[Ca^{2+}] = 0.1\ \mu M$, and the corresponding latencies for the first opening of any channel among a population of 50 IP_3R channels (i.e., the predicted puff latency) (*B*). (*C* and *D*) Corresponding dependence of mean single-channel first-opening latency (*C*) and puff latency (*D*) for a cluster of 50 channels as a function of $[Ca^{2+}]$ for $[IP_3]_{Stim} = 10\mu M$ (*stars*) and $[IP_3]_{Stim} = 0.1\mu M$ (*squares*).

The results are depicted graphically in Fig. 8 *C* by contours of increasing Θ. Here we discuss the optimal function Θ by varying both the channel number N in the cluster and the resting Ca^{2+} concentration. The resting Ca^{2+} concentration in cytosol is ~0.05–0.2 μM. An optimal region in the N-$[Ca^{2+}]_{Rest}$ plane obtained with the model also centered at $[Ca^{2+}]_{Rest} = 0.12\ \mu M$ with $N = 55$. Our simulation given in Fig. 8 *C* suggests that the total channel number in a cluster may be in the range of 40 to 70 (considering the contour of $\Theta = 2.0$ where $[Ca^{2+}]_{Rest}$ is in the biologically realistic range of 0.05 to 0.2 μM).

Effect of reduced triggering probability on puff latency

In the above discussion, the puff latency was calculated assuming that the first opening of any single channel in a cluster invariably triggers a puff by CICR. However, it is likely that brief channel openings may provide insufficient ''trigger'' calcium to initiate a puff. We thus explored the effect of reducing the probability of puff initiation by reducing the probability, $P_{Trigger}$, that any given channel opening triggers a puff. Specifically, if the first opening of a channel within a cluster failed to trigger a puff, we then checked whether the next opening event (of the same or a different channel) triggered a puff with the same $P_{Trigger}$, and so on, until a puff was evoked.

Our simulation shows that the average puff latency varies only slightly as a function of trigger probability, $P_{Trigger}$, for $P_{Trigger} \geq 30\%$. For example, the predicted cluster number N giving a good fit to the experimental data remained at ~50 for $P_{Trigger} > 50\%$, increasing to $N = 70$ for $P_{Trigger} = 30\%$ and $N = 100$ for $P_{Trigger} = 20\%$.

DISCUSSION

We propose a dynamic model of the type-1 IP_3 receptor in *Xenopus* oocytes, with the long-term goal of applying the model for stochastic simulations of cellular Ca^{2+} signaling dynamics within a realistic cytosolic environment. We specifically model the *Xenopus* oocyte system, as this is the subject of numerous cellular imaging studies (6–8,29) and a wealth of data are available from patch-clamp experiments on oocyte nuclear IP_3R (9–12).

Our model assumes that each IP_3R channel is comprised of four identical and independent subunits. Like the De Young-Keizer model (14), each subunit consists of two independent Ca^{2+}-binding sites—an activating and an inhibitory binding site—and one IP_3 binding site. Furthermore, we assume that a subunit becomes ''active'' after a conformational change that occurs after both IP_3-binding sites and the activating, but not the inhibitory, Ca^{2+}-binding sites are occupied. The channel is open when at least three subunits are in the active state. The model provides a good fit to steady-state experimental data of channel-open probability P_O $[IP_3]$ (10,11), although it predicts a bell-shaped curve with $[Ca^{2+}]$ even at high concentrations of IP_3, different from the ''flat-topped'' relationship obtained by Mak et al. (11) and Baran (20). Moreover, the model accounts well for the observed distributions of channel-open and -closed dwell times.

With the parameters given in Table 1, our model assumes that there is a negative allosteric interaction between the IP_3 site and the inhibitory Ca^{2+} site, i.e., IP_3 binding reduces the affinity of the inhibitory Ca^{2+} site (from K_4 to K_2), and Ca^{2+} binding to the inhibitory site decreases the affinity of the IP_3 site (from K_1 to K_3). The affinity of the activating Ca^{2+} sites is independent of the inhibitory Ca^{2+}-binding and IP_3-binding sites.

In this article, we restrict consideration of the IP_3R model to situations where the Ca^{2+} concentration remains constant; the effects of feedback by Ca^{2+} flux through the channel will be considered in future publications. Nevertheless, the results provide novel insights into the functioning of both individual IP_3Rs and the population behavior of clusters of IP_3Rs at puff sites.

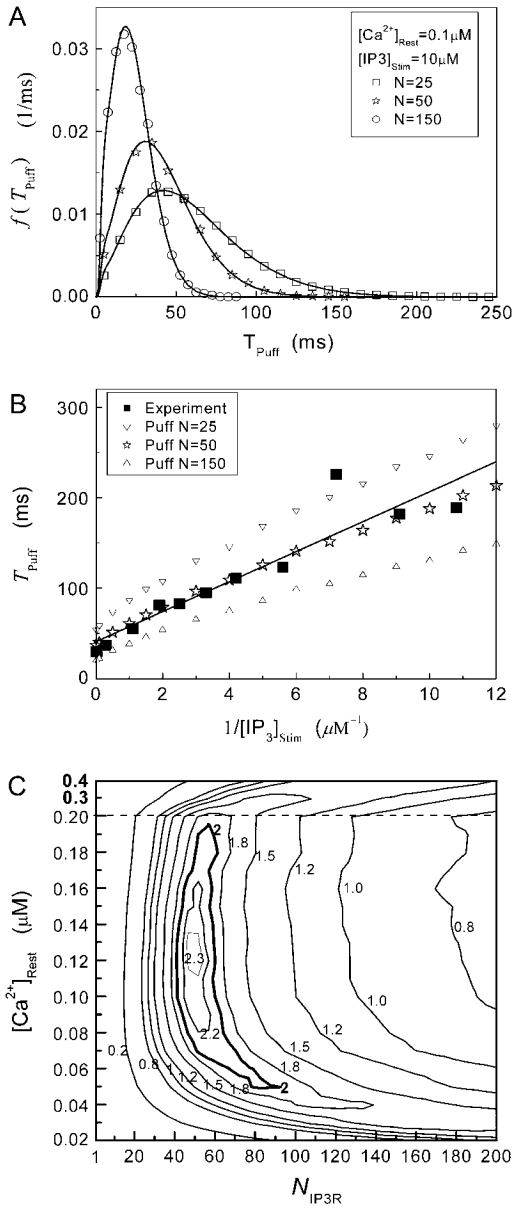

FIGURE 8 Simulation and experimental measurements of puff latencies. (*A*) Predicted latency distribution of puffs for $[IP_3]_{Stim} = 10\ \mu M$ and $[Ca^{2+}]_{Rest} = 0.1\ \mu M$, assuming that a puff is evoked by the first opening of any IP_3R channel within clusters containing N IP_3Rs. The open symbols are for stochastic simulation results with $N = 25$ (*inverted triangles*), 50 (*stars*), or 150 (*triangles*). The corresponding solid curves are obtained from the transition matrix theory. (*B*) Predicted mean puff latencies as functions of $[IP_3]_{Stim}$ are shown for clusters containing $N = 25$ (*inverted triangles*), 50 (*stars*), and 150 (*triangles*) channels, with $[Ca^{2+}]_{Rest} = 0.1\ \mu M$. For comparison, experimental data of puff latencies as a function of $[IP_3]$ step is replotted as solid squares from Callamaras et al. (7) and Parker et al. (8) after normalizing as described in the text. (*C*) Goodness of fit of stochastic simulations to the experimental data as functions of both the number of IP_3R in a cluster and the resting Ca^{2+} concentration. Optimal agreement (maximal value of the index Θ) is obtained with $N \approx 40$–70 and $[Ca^{2+}]_{Rest} \approx 0.05$–$0.2\ \mu M$.

Channel opening by three out of four subunits

As is the case for numerous ion channels, the IP_3R is a multimer formed from several subunits. In some instances, exemplified by AMPA receptors (24), the single-channel conductance increases in a stepwise fashion as more subunits become active after binding of ligand. However, the *Xenopus* oocyte IP_3R displays only a single major conductance level (11,12), and our model correspondingly incorporates only a single open state. The question then arises as to how many of the four subunits must be active to open the channel.

We assume that the channel is open when either three or four subunits are in an ''active'' state. This assumption has previously been applied in some IP_3R models (23), and we also assume that there is only one conductance state, irrespective of whether three or four subunits are active. An alternative approach to our simple model has been used in allosteric modeling of the tetrameric IP_3 and ryanodine receptors (11,30). Such allosteric models are extremely complex because they consider different conductance state with different open probability corresponding to different number of subunits in the active state, which will involve numerous free parameters and be difficult to implement in stochastic simulations. The simulation shows that our simple IP_3R model can successfully reproduce two levels of experimental data obtained from patch-clamp of nuclear IP_3R and confocal imaging of clustered IP_3Rs.

One important consequence of assuming that channel openings occur with either three or four subunits in the active state is that this model successfully predicts the dependence of open dwell time on ligand concentrations, whereas if the channel opening requires all four active subunits to be in the active state, a ligand-independent, constant open dwell time would be expected, since the open time depends only on the backward rate constant b_0. The ligand dependence of mean open time can be intuitively understood by distinguishing two types of channel-open state, those involving only three active subunits (A3-only), and those involving four active subunits (A4-related). The mean dwell times in each state are relatively independent of ligand concentration, but A4-related openings are much longer than A3-only openings, since channel closure requires two subunits, rather than just one, to become inactive. Changes in mean channel open time thus derive from changes in the proportion of A3-only and A4-related openings. For example, at very low and very high $[Ca^{2+}]$ the probability of subunits becoming active is small, so almost all channel openings involve only three active subunits and the mean open time thus corresponds to the A3-only dwell time (~4 ms; Fig. 3 *B*). Conversely, at optimal $[Ca^{2+}]$ one half of all openings are A4-related, so the channel open time is given by the average of the A3-only and A4-related dwell times (~9 ms).

The existence of distinct A3-only and A4-related openings may also explain experimental observations that the distributions of mean IP_3R channel open times follow two

exponential components (12). Mak et al. (12) proposed that these components arise from two kinetically distinguishable open states with different time constants, but our model suggests that they may instead reflect the different mean dwell times of A3-only and A4-related openings.

Furthermore, our model indicates a complex situation for the closed-time distribution. In principle, there are 486 distinct closed states and 9 distinct open states (J. Shuai, I. Parker, and J. E. Pearson; unpublished), but in practice, only two or three major exponential components can be discriminated from experimental or stochastic simulation data. The faster component primarily reflects brief closings caused by any one of the three active subunits undergoing multiple transitions between the active A-state and the inactive (110) state, whereas the slower components involve ligand binding transitions.

Inactivation of IP_3R at basal cytosolic $[Ca^{2+}]$

One feature of the model is that the dissociation constant of the inhibitory Ca^{2+} binding site increases enormously from $K_4 = 0.072\ \mu M$ to $K_2 = 16\ \mu M$ after binding of IP_3. This scheme is concordant with the conclusion of Mak et al. (10) that the effect of IP_3 binding is not to directly activate the channel, as generally assumed, but rather to relieve the channel from Ca^{2+} inhibition. A distinction, however, is that whereas Mak et al. (10) proposed that the sole action of IP_3 is to reduce the effective affinity of the inhibitory Ca^{2+}-binding site, in our model it plays an additional role as an obligate agonist. That is to say, channel opening cannot occur in the absence of IP_3 even if the inhibitory Ca^{2+} sites are unoccupied and the activating sites bind Ca^{2+} (11).

An important consequence of the high affinity of the inhibitory Ca^{2+} binding in the absence of IP_3 is that a surprisingly high proportion of IP_3R are predicted to be in a Ca^{2+}-inhibited state under basal resting cytosolic conditions with zero $[IP_3]$. For example, with $[Ca^{2+}]_{Rest} = 0.1\ \mu M$, ~60% of subunits would be Ca^{2+}-inhibited, resulting in ~82% of IP_3R having two or more subunits in an inhibited state so that the channel cannot immediately open on binding of IP_3 and activating Ca^{2+}. Thus, the latency of Ca^{2+} responses evoked by a step increase of $[IP_3]$ will depend strongly on the dissociation of Ca^{2+} from inhibitory sites, as well the rates of association of Ca^{2+} and IP_3 to activating sites. This is evident in Fig. 7 *C*, where the mean first-opening latency of a single IP_3R initially shortens as $[Ca^{2+}]_{Rest}$ is raised from a low value (0.005 μM), but reaches a minimum at ~0.05 μM and thereafter actually shows a slight lengthening in response to $[IP_3]_{Stim} = 0.1\ \mu M$. An explanation is that binding of Ca^{2+} to activating sites is rate-limiting at very low $[Ca^{2+}]_{Rest}$, but that at biological concentrations of $[Ca^{2+}]_{Rest}$ there is an increasing likelihood of subunits being in an inhibited state so that the latency approaches a minimal value set by the dissociation rate b_2 from inhibitory Ca^{2+}-binding sites. Moreover, the magnitude of Ca^{2+} release will depend on the available fraction of noninactivated IP_3R, which in turn will be a function of the resting $[Ca^{2+}]$ before stimulation.

Number of IP_3R at a puff site

Finally, we extrapolated our model from the individual IP_3R to consider the latency of puffs generated by clusters containing multiple IP_3Rs. On the assumptions that IP_3Rs within a cluster are independent and that a puff is triggered by whichever channel in the cluster is the first to open, we obtained an optimal fit to experimental measurements of puff latency as a function of $[IP_3]$ (7,8) for clusters containing $N =$ 40–70 IP_3Rs. This result is affected only slightly by changes of assumed resting Ca^{2+} concentration within a biologically realistic range of 0.05–0.2 μM.

The conclusion that clusters contain 40–70 IP_3Rs likely represents a minimal estimate, since very brief channel openings may fail to initiate a puff, thereby requiring the number of IP_3Rs in the model cluster to be increased to match the experimental data. However, this effect becomes appreciable only if the triggering probability is quite low. For example, our simulation shows that if channel openings have a 50% or better chance of initiating a puff ($P_{Trigger} > 50\%$), a cluster size with $N \sim 50$ still gives a good fitting to the experimental data of puff latency. At smaller $P_{Trigger}$, larger values of N are required to obtain a good fit to the experimental data; for example $N =$ 70 for $P_{Trigger} = 30\%$. This treatment is simplified compared to the biological situation, where calcium lingering from a channel opening that failed to trigger a puff would likely increase the probability of a subsequent opening to trigger a puff. However, in our simulation, for simplicity, we assume that all the opening events for all the channels in the cluster has the same probability $P_{Trigger}$ to trigger a puff; and that the resting calcium concentration is always fixed no matter how many opening channels failed to trigger a puff. We plan to address this question more fully in a future study by considering the stochastic dynamics of clustered channels, incorporating the feedback of released Ca^{2+} ions.

It should be noted that these values estimate the total number of IP_3Rs clustered at a puff site. In contrast, most experimental work has used measurements of puff amplitudes to estimate the number of open IP_3R channels that contribute to the Ca^{2+} flux during a puff. For example, we recently capitalized on the discovery of ''trigger'' events that may represent the opening of a single IP_3R channel that initiates a puff (31) to construct a deterministic puff model that predicts the involvement of some 25–35 open channels (29). Thus, it is likely that only a minority of IP_3Rs in a cluster open during a puff, as is expected if many receptors are inactivated at resting cytosolic $[Ca^{2+}]$ and Ca^{2+} dissociates from inhibitory binding sites only slowly on the timescale of puff latencies (a few hundred milliseconds or shorter).

This work was supported by National Institutes of Health grants GM 65830 and GM48071.

REFERENCES

1. Foskett, J. K., C. White, K. Cheung, and D. D. Mak. 2007. Inositol trisphosphate receptor Ca^{2+} release channels. *Physiol. Rev.* 87:593–658.
2. Taylor, C. W., P. C. da Fonseca, and E. P. Morris. 2004. IP_3 receptors: the search for structure. *Trends Biochem. Sci.* 29:210–219.
3. Bosanac, I., J. R. Alattia, T. K. Mal, J. Chan, S. Talarico, F. K. Tong, K. I. Tong, F. Yoshikawa, T. Furuichi, M. Iwai, T. Michikawa, K. Mikoshiba, and M. Ikura. 2002. Structure of the inositol 1,4,5-trisphosphate receptor binding core in complex with its ligand. *Nature.* 420:696–700.
4. Bezprozvanny, I. 2005. The inositol 1,4,5-trisphosphate receptors. *Cell Calcium.* 38:261–272.
5. Bezprozvanny, I., J. Watras, and B. E. Ehrlich. 1991. Bell-shaped calcium-response curves of $Ins(1,4,5)P_3$- and calcium-gated channels from endoplasmic reticulum of cerebellum. *Nature.* 351:751–754.
6. Yao, Y., J. Choi, and I. Parker. 1995. Quantal puffs of intracellular Ca^{2+} evoked by inositol trisphosphate in *Xenopus* oocytes. *Journal of Physiology-London.* 482:533–553.
7. Callamaras, N., J. S. Marchant, X. P. Sun, and I. Parker. 1998. Activation and co-ordination of $InsP_3$-mediated elementary Ca^{2+} events during global Ca^{2+} signals in *Xenopus* oocytes. *Journal of Physiology-London.* 509:81–91.
8. Parker, I., Y. Yao, and V. Ilyin. 1996. Fast kinetics of calcium liberation induced in *Xenopus* oocytes by photoreleased inositol trisphosphate. *Biophys. J.* 70:222–237.
9. Mak, D. O., and J. K. Foskett. 1994. Single-channel inositol 1,4,5-trisphosphate receptor currents revealed by patch clamp of isolated *Xenopus* oocyte nuclei. *J. Biol. Chem.* 269:29375–29378.
10. Mak, D. O., S. McBride, and J. K. Foskett. 1998. Inositol 1,4,5-trisphosphate activation of inositol trisphosphate receptor Ca^{2+} channel by ligand tuning of Ca^{2+} inhibition. *Proc. Natl. Acad. Sci. USA.* 95: 15821–15825.
11. Mak, D. O., S. M. McBride, and J. K. Foskett. 2003. Spontaneous channel activity of the inositol 1,4,5-trisphosphate ($InsP_3$) receptor ($InsP_3R$). Application of allosteric modeling to calcium and $InsP_3$ regulation of $InsP_3R$ single-channel gating. *J. Gen. Physiol.* 122:583–603.
12. Mak, D. O., and J. K. Foskett. 1997. Single-channel kinetics, inactivation, and spatial distribution of inositol trisphosphate (IP_3) receptors in *Xenopus* oocyte nucleus. *J. Gen. Physiol.* 109:571–587.
13. Atri, A., J. Amundson, D. Clapham, and J. Sneyd. 1993. A single-pool model for intracellular calcium oscillations and waves in the *Xenopus laevis* oocyte. *Biophys. J.* 65:1727–1739.
14. De Young, G. W., and J. Keizer. 1992. A single-pool inositol 1,4,5-trisphosphate-receptor-based model for agonist-stimulated oscillations in Ca^{2+} concentration. *Proc. Natl. Acad. Sci. USA.* 89:9895–9899.
15. Kaftan, E. J., B. E. Ehrlich, and J. Watras. 1997. Inositol 1,4,5-trisphosphate ($InsP_3$) and calcium interact to increase the dynamic range of $InsP_3$ receptor-dependent calcium signaling. *J. Gen. Physiol.* 110:529–538.
16. Sneyd, J., and J. F. Dufour. 2002. A dynamic model of the type-2 inositol trisphosphate receptor. *Proc. Natl. Acad. Sci. USA.* 99:2398–2403.
17. Swillens, S., P. Champeil, L. Combettes, and G. Dupont. 1998. Stochastic simulation of a single inositol 1,4,5-trisphosphate-sensitive Ca^{2+} channel reveals repetitive openings during ''blip-like'' Ca^{2+} transients. *Cell Calcium.* 23:291–302.
18. Fraiman, D., and S. P. Dawson. 2004. A model of the IP_3 receptor with a luminal calcium binding site: stochastic simulations and analysis. *Cell Calcium.* 35:403–413.
19. Sneyd, J., and M. Falcke. 2005. Models of the inositol trisphosphate receptor. *Prog. Biophys. Mol. Biol.* 89:207–245.
20. Baran, I. 2003. Integrated luminal and cytosolic aspects of the calcium release control. *Biophys. J.* 84:1470–1485.
21. Hille, B. 2001: Ion Channels of Excitable Membranes, 3rd ed. Sinauer Associates, Sunderland, MA.
22. Adkins, C. E., and C. W. Taylor. 1999. Lateral inhibition of inositol 1,4,5-trisphosphate receptors by cytosolic Ca(2+). *Curr. Biol.* 9:1115–1118.
23. Falcke, M., L. Tsimring, and H. Levine. 2000. Stochastic spreading of intracellular Ca^{2+} release. *Physical Review E.* 62:2636–2643.
24. Rosenmund, C., Y. Stern-Bach, and C. F. Stevens. 1998. The tetrameric structure of a glutamate receptor channel. *Science.* 280:1596–1599.
25. Bruno, W. J., J. Yang, and J. E. Pearson. 2005. Using independent open-to-closed transitions to simplify aggregated Markov models of ion channel gating kinetics. *Proc. Natl. Acad. Sci. USA.* 102:6326–6331.
26. Yang J., W. J. Bruno, W. S. Hlavacek, and J. E. Pearson. 2006. On imposing detailed balance in complex reaction mechanisms. *Biophys. J.* 91:1136–1141.
27. Shuai, J. W., and P. Jung. 2002. Stochastic properties of Ca^{2+} release of inositol 1,4,5-trisphosphate receptor clusters. *Biophys. J.* 83:87–97.
28. Shuai, J. W., and P. Jung. 2003. Optimal ion channel clustering for intracellular calcium signaling. *Proc. Natl. Acad. Sci. USA.* 100: 506–510.
29. Rose, H. J., S. Dargan, J. Shuai, and I. Parker. 2006. ''Trigger'' events precede calcium puffs in *Xenopus* oocytes. *Biophys. J.* 91:4024–4032.
30. Zahradnik, I., S. Gyorke, and A. Zahradnikova. 2005. Calcium activation of ryanodine receptor channels–reconciling RyR gating models with tetrameric channel structure. *J. Gen. Physiol.* 126:515–527.
31. Shuai, J., H. J. Rose, and I. Parker. 2006. The number and spatial distribution of IP_3 receptors underlying calcium puffs in *Xenopus* oocytes. *Biophys. J.* 91:4033–4044.